We are IntechOpen, the world's leading publisher of Open Access books Built by scientists, for scientists

6,900
Open access books available

186,000
International authors and editors

200M
Downloads

Our authors are among the

154
Countries delivered to

TOP 1%
most cited scientists

12.2%
Contributors from top 500 universities

CLARIVATE ANALYTICS
BOOK CITATION INDEX
INDEXED

WEB OF SCIENCE™

Selection of our books indexed in the Book Citation Index
in Web of Science™ Core Collection (BKCI)

Interested in publishing with us?
Contact book.department@intechopen.com

Numbers displayed above are based on latest data collected.
For more information visit www.intechopen.com

Parametric Vibration Analysis of Transmission Mechanisms Using Numerical Methods

Nguyen Van Khang and Nguyen Phong Dien

Additional information is available at the end of the chapter

1. Introduction

Transmission mechanisms are frequently used in machines for power transmission, variation of speed and/or working direction and conversion of rotary motion into reciprocating motion. At high speeds, the vibration of mechanisms causes wear, noise and transmission errors. The vibration problem of transmission mechanisms has been investigated for a long time, both theoretically and experimentally. In dynamic modelling, a transmission mechanism is usually modelled as a multibody system. The differential equations of motion of a multibody system that undergo large displacements and rotations are fully nonlinear in n generalized coordinates in vector of variable q [1–4].

$$M(q, t)\ddot{q} + k(\dot{q}, q, t) = h(\dot{q}, q, t) \tag{1}$$

It is very difficult or impossible to find the solution of Eq. (1) with the analytical way. Nevertheless, the numerical methods are efficient to solve the problem [5-9].

Besides, many technical systems work mostly on the proximity of an equilibrium position or, especially, in the neighbourhood of a desired motion which is usually called "programmed motion", "desired motion", "fundamental motion", "input–output motion" and etc. according to specific problems. In this chapter, the term "desired fundamental motion" is used for this object. The desired fundamental motion of a robotic system, for instance, is usually described through state variables determined by prescribed motions of the end-effector. For a mechanical transmission system, the desired fundamental motion can be the motion of working components of the system, in which the driver output rotates uniformly and all components are assumed to be rigid. It is very convenient to linearize the equa-

tions of motion about this configuration to take advantage of the linear analysis tools [10-18]. In other words, linearization makes it possible to use tools for studying linear systems to analyze the behavior of multibody systems in the vicinity of a desired fundamental motion. For this reason, the linearization of the equations of motion is most useful in the study of control [12-13], machinery vibrations [14-19] and the stability of motion [20-21]. Mathematically, the linearized equations of motion of a multibody system form usually a set of linear differential equations with time-varying coefficients. Considering steady-state motions of the multibody system only, one obtains a set of linear differential equations having time-periodic coefficients.

$$M(t)\ddot{q}(t) + C(t)\dot{q}(t) + K(t)q(t) = d(t) \tag{2}$$

Note that Eq. (2) can be expressed in the compact form as

$$\dot{x} = P(t)x + f(t) \tag{3}$$

where we use the state variable x

$$x = \begin{bmatrix} q \\ \dot{q} \end{bmatrix}, \ \dot{x} = \begin{bmatrix} \dot{q} \\ \ddot{q} \end{bmatrix} \tag{4}$$

and the matrix of coefficients $P(t)$, vector $f(t)$ are defined by

$$P(t) = \begin{bmatrix} 0 & I \\ -M^{-1}K & -M^{-1}C \end{bmatrix}, \ f(t) = \begin{bmatrix} 0 \\ M^{-1}d \end{bmatrix}, \tag{5}$$

where I denotes the $n \times n$ identity matrix.

In the steady state of a machine, the working components perform stationary motions [14-18], matrices $M(t)$, $C(t)$, $K(t)$ and vector $d(t)$ in Eq. (2) are time-periodic with the least period T. Hence, Eq. (2) represents a parametrically excited system. For calculating the steady-state periodic vibrations of systems described by differential equations (1) or (2) the harmonic balance method, the shooting method and the finite difference method are usually used [8,11,14]. In addition, the numerical integration methods as Newmark method and Runge-Kutta method can also be applied to calculate the periodic vibration of parametric vibration systems governed by Eq. (2) [5-9].

Since periodic vibrations are a commonly observed phenomenon of transmission mechanisms in the steady-state motion, a number of methods and algorithms were developed to find a T-periodic solution of the system described by Eq. (2). A common approach is by imposing an arbitrary set of initial conditions, and solving Eq. (2) in time using numerical methods until the transient term of the solution vanishes and only the periodic steady-state solution remains [14,22]. Besides, the periodic solution can be found directly by other speci-

alized techniques such as the harmonic balance method, the method of conventional oscillator, the WKB method [14-16, 23, 24].

Following the above introduction, an overview of the numerical calculation of dynamic stability conditions of linear dynamic systems with time-periodic coefficients is presented in Section 2. Sections 3 presents numerical procedures based on Runge-Kutta method and Newmark method to find periodic solutions of linear systems with time-periodic coefficients. In Section 4, the proposed approach is demonstrated and validated by dynamic models of transmission mechanisms and measurements on real objects. The improvement in the computational efficiency of Newmark method comparing with Runge-Kutta method for linear systems is also discussed.

2. Numerical calculation of dynamic stability conditions of linear dynamic systems with time-periodic coefficients: An overview

We shall consider a system of homogeneous differential equations

$$\dot{x} = P(t)x \tag{6}$$

where $P(t)$ is a continuous T-periodic $n \times n$ matrix. According to Floquet theory [17, 18, 20, 21], the characteristic equation of Eq. (6) is independent of the chosen fundamental set of solutions. Therefore, the characteristic equation can be formulated by the following way. Firstly, we specify a set of n initial conditions $x_i(0)$ for $i = 1, ..., n$, their elements

$$x_i^{(s)}(0) = \begin{cases} 1 & \text{when } s = i \\ 0 & \text{otherwhile} \end{cases} \tag{7}$$

and $[x_1(0), x_2(0), ..., x_n(0)] = I$. By implementing numerical integration of Eq. (6) within interval $[0, T]$ for n given initial conditions respectively, we obtain n vectors $x_i(T)$, $i = 1, ..., n$. The matrix $\Phi(t)$ defined by

$$\Phi(T) = [x_1(T), x_2(T), ..., x_n(T)] \tag{8}$$

is called the monodromy matrix of Eq. (6) [20]. The characteristic equation of Eq. (6) can then be written in the form

$$\left|\mathbf{\Phi}(T) - \rho\mathbf{I}\right| = \begin{vmatrix} x_1^{(1)}(T) - \rho & x_2^{(1)}(T) & .... & x_n^{(1)}(T) \\ x_1^{(2)}(T) & x_2^{(2)}(T) - \rho & .... & x_n^{(2)}(T) \\ .... & .... & .... & .... \\ x_1^{(n)}(T) & x_2^{(n)}(T) & .... & x_n^{(n)}(T) - \rho \end{vmatrix} = 0 \qquad (9)$$

Expansion of Eq. (9) yields a n-order algebraic equation

$$\rho^n + a_1\rho^{n-1} + a_2\rho^{n-2} + ... + a_{n-1}\rho + a_n = 0 \qquad (10)$$

where unknowns $\rho_k (k = 1, ..., n)$, called Floquet multipliers, can be determined from Eq. (10). Floquet exponents are given by

$$\lambda_k = \frac{1}{T}\ln\rho_k, \ (k = 1, ..., n) \qquad (11)$$

When the Floquet multipliers or Floquet exponents are known, the stability conditions of solutions of the system of linear differential equations with periodic coefficients can be easily determined according to the Floquet theorem [17–20]. The concept of stability according to Floquet multipliers can be expressed as follows.

If $|\rho_k| 1$, the trivial solution $x = 0$ of Eq. (6) will be asymptotically stable. Conversely, the solution $x = 0$ of Eq. (6) becomes unstable if at least one Floquet multiplier has modulus being larger than 1.

If $|\rho_k| \leq 1$ and Floquet multipliers with modulus 1 are single roots of the characteristic equation, the solution $x = 0$ of Eq. (6) is stable.

If $|\rho_k| \leq 1$ and Floquet multipliers with modulus 1 are multiple roots of the characteristic equation, and the algebraic multiplicity is equal to their geometric multiplicity, then the solution $x = 0$ of Eq. (6) is also stable.

3. Numerical procedures for calculating periodic solutions of linear dynamic systems with time-periodic coefficients

3.1. Numerical procedure based on Runge-Kutta method

Now we consider only the periodic vibration of a dynamic system which is governed by a set of linear differential equations with periodic coefficients. As already mentioned in the previous section, these differential equations can be expressed in the compact matrix form

$$\dot{x} = P(t)x + f(t) \tag{12}$$

where x is the vector of state variables, matrix $P(t)$ and vector $f(t)$ are periodic in time with period T. The system of homogeneous differential equations corresponding to Eq. (12) is

$$\dot{x} = P(t)x \tag{13}$$

As well known from the theory of differential equations, if Eq. (13) has only non-periodic solutions except the trivial solution, then Eq. (12) has an unique T-periodic solution. This periodic solution can be obtained by choosing the appropriate initial condition for the vector of variables x and then implementing numerical integration of Eq. (12) within interval $[0, T]$. An algorithm is developed to find the initial value for the periodic solution [18, 19]. Firstly, the T-periodic solution must satisfy the following condition

$$x(0) = x(T) \tag{14}$$

The interval $[0, T]$ is now divided into m equal subintervals with the step-size $h = t_i - t_{i-1} = T/m$. At the discrete times t_i and t_{i+1}, $x_i = x(t_i)$ and $x_{i+1} = x(t_{i+1})$ represent the states of the system, respectively. Using the fourth-order Runge-Kutta method, we get a numerical solution [5]

$$x_i = x_{i-1} + \frac{1}{6}\left[k_1^{(i-1)} + 2k_2^{(i-1)} + 2k_3^{(i-1)} + k_4^{(i-1)}\right] \tag{15}$$

where

$$
\begin{aligned}
k_1^{(i-1)} &= h\left[P(t_{i-1})x_{i-1} + f(t_{i-1})\right], \\
k_2^{(i-1)} &= h\left[P(t_{i-1} + \frac{h}{2})(x_{i-1} + \frac{1}{2}k_1^{(i-1)}) + f(t_{i-1} + \frac{h}{2})\right], \\
k_3^{(i-1)} &= h\left[P(t_{i-1} + \frac{h}{2})(x_{i-1} + \frac{1}{2}k_2^{(i-1)}) + f(t_{i-1} + \frac{h}{2})\right], \\
k_4^{(i-1)} &= h\left[P(t_i)(x_{i-1} + k_3^{(i-1)}) + f(t_i)\right].
\end{aligned}
\tag{16}
$$

Substituting Eq. (16) into Eq. (15), we obtain

$$x_i = A_{i-1}x_{i-1} + b_{i-1} \tag{17}$$

where matrix A_{i-1} is given by

$$
\begin{aligned}
A_{i-1} = I + \frac{1}{6}\Big\{ & h\Big[P(t_{i-1}) + 4P(t_{i-1} + \frac{h}{2}) + P(t_i)\Big] \\
& + h^2\Big[P(t_{i-1} + \frac{h}{2})P(t_{i-1}) + P^2(t_{i-1} + \frac{h}{2}) + \frac{1}{2}P(t_i)P(t_{i-1} + \frac{h}{2})\Big] \\
& + \frac{h^3}{2}\Big[P^2(t_{i-1} + \frac{h}{2})P(t_{i-1}) + \frac{1}{2}P(t_i)P^2(t_{i-1} + \frac{h}{2})\Big] \\
& + \frac{h^4}{4}P(t_i)P^2(t_{i-1} + \frac{h}{2})P(t_{i-1})\Big\} (i = 1, \, ..., \, m),
\end{aligned}
\tag{18}
$$

and vector b_{i-1} takes the form

$$
\begin{aligned}
b_{i-1} = \frac{1}{6}\Big\{ & h\Big[f(t_{i-1}) + 4f(t_{i-1} + \frac{h}{2}) + f(t_i)\Big] \\
& + h^2\Big[P(t_{i-1} + \frac{h}{2})f(t_{i-1}) + P(t_{i-1} + \frac{h}{2})f(t_{i-1} + \frac{h}{2}) + \frac{1}{2}P(t_i)f(t_{i-1} + \frac{h}{2})\Big] \\
& + \frac{h^3}{2}\Big[P^2(t_{i-1} + \frac{h}{2})f(t_{i-1}) + P(t_i)P(t_{i-1} + \frac{h}{2})f(t_{i-1} + \frac{h}{2})\Big] \\
& + \frac{h^4}{4}P(t_i)P^2(t_{i-1} + \frac{h}{2})f(t_{i-1})\Big\}.
\end{aligned}
\tag{19}
$$

Expansion of Eq. (17) for $i = 1$ to m yields

$$
\begin{aligned}
x_1 &= A_0 x_0 + c_1 \\
x_2 &= A_1 A_0 x_0 + c_2 \\
& \cdots\cdots\cdots\cdots\cdots\cdots \\
x_m &= \Big(\prod_{i=m-1}^{0} A_i\Big)x_0 + c_m
\end{aligned}
\tag{20}
$$

where $c_0 = 0$, $c_1 = A_0 c_0 + b_0$, $c_2 = A_1 c_1 + b_1$,..., $c_m = A_{m-1}c_{m-1} + b_{m-1}$. Using the boundary condition according to Eq. (14), the last equation of Eq. (20) yields a set of the linear algebraic equations

$$
\Big(I - \prod_{i=m-1}^{0} A_i\Big)x_0 = c_m.
\tag{21}
$$

The solution of Eq. (21) gives us the initial value for the periodic solution of Eq. (12). Finally, the periodic solution of Eq. (12) with the corresponding initial value can be calculated using the computational scheme according to Eq. (15).

3.2. Numerical procedure based on Newmark integration method

The procedure presented below for finding the T-periodic solution of Eq. (2) is based on the Newmark direct integration method. Firstly, the interval $[0, T]$ is also divided into m equal subintervals with the step-size $h = t_i - t_{i-1} = T / m$. We use notations $q_i = q(t_i)$ and $q_{i+1} = q(t_{i+1})$ to represent the solution of Eq. (2) at discrete times t_i and t_{i+1} respectively. The T-periodic solution must satisfy the following conditions

$$q(0) = q(T), \ \dot{q}(0) = \dot{q}(T), \ \ddot{q}(0) = \ddot{q}(T). \tag{22}$$

Based on the single-step integration method proposed by Newmark, we obtain the following approximation formulas [6-7]

$$q_{i+1} = q_i + h \dot{q}_i + h^2 \left(\frac{1}{2} - \beta \right) \ddot{q}_i + \beta h^2 \ddot{q}_{i+1}, \tag{23}$$

$$\dot{q}_{i+1} = \dot{q}_i + (1-\gamma)h \ddot{q}_i + \gamma h \ddot{q}_{i+1}, \tag{24}$$

Constants β, γ are parameters associated with the quadrature scheme. Choosing $\gamma = 1/4$ and $\beta = 1/6$ leads to linear interpolation of accelerations in the time interval $[t_i, t_{i+1}]$. In the same way, choosing $\gamma = 1/2$, $\beta = 1/4$ corresponds to considering the acceleration average value over the time interval [6, 7].

From Eq. (2) we have the following iterative computational scheme at time t_{i+1}

$$M_{i+1}\ddot{q}_{i+1} + C_{i+1}\dot{q}_{i+1} + K_{i+1}q_{i+1} = d_{i+1}, \tag{25}$$

where $M_{i+1} = M(t_{i+1})$, $C_{i+1} = C(t_{i+1})$, $K_{i+1} = K(t_{i+1})$ and $d_{i+1} = d(t_{i+1})$.

In the next step, substitution of Eqs. (23) and (24) into Eq. (25) yields

$$\left(M_{i+1} + \gamma h \, C_{i+1} + \beta h^2 K_{i+1}\right)\ddot{q}_{i+1} = d_{i+1} - C_{i+1}[\dot{q}_i + (1-\gamma)h \ddot{q}_i] - K_{i+1}\left[q_i + h \dot{q}_i + h^2 \left(\frac{1}{2} - \beta \right) \ddot{q}_i\right]. \tag{26}$$

The use of Eqs. (23) and (24) leads to the prediction formulas for velocities and displacements at time t_{i+1}

$$q_{i+1}^* = q_i + h \dot{q}_i + h^2 \left(\frac{1}{2} - \beta \right) \ddot{q}_i, \ \dot{q}_{i+1}^* = \dot{q}_i + (1-\gamma)h \ddot{q}_i. \tag{27}$$

Eq. (27) can be expressed in the matrix form as

$$\begin{bmatrix} \mathbf{q}_{i+1}^* \\ \dot{\mathbf{q}}_{i+1}^* \end{bmatrix} = \mathbf{D} \begin{bmatrix} \mathbf{q}_i \\ \dot{\mathbf{q}}_i \\ \ddot{\mathbf{q}}_i \end{bmatrix} \tag{28}$$

with

$$D = \begin{bmatrix} I & h\,I & h^2(0.5-\beta)I \\ 0 & I & (1-\gamma)h\,I \end{bmatrix} \tag{29}$$

where $\mathbf{0}$ represents the $n \times n$ matrix of zeros. Eq. (26) can then be rewritten in the matrix form as

$$\ddot{\mathbf{q}}_{i+1} = \left(\mathbf{S}_{i+1}\right)^{-1} \mathbf{d}_{i+1} - \left(\mathbf{S}_{i+1}\right)^{-1} \mathbf{H}_{i+1} \begin{bmatrix} \mathbf{q}_{i+1}^* \\ \dot{\mathbf{q}}_{i+1}^* \end{bmatrix}, \tag{30}$$

where matrices S_{i+1} and H_{i+1} are defined by

$$S_{i+1} = M_{i+1} + \gamma h\,C_{i+1} + h^2 \beta K_{i+1}, \tag{31}$$

$$H_{i+1} = \begin{bmatrix} K_{i+1} & C_{i+1} \end{bmatrix}. \tag{32}$$

By substituting relationships (28) into (30) we find

$$\ddot{\mathbf{q}}_{i+1} = \left(\mathbf{S}_{i+1}\right)^{-1} \mathbf{d}_{i+1} - \left(\mathbf{S}_{i+1}\right)^{-1} \mathbf{H}_{i+1} \mathbf{D} \begin{bmatrix} \mathbf{q}_i \\ \dot{\mathbf{q}}_i \\ \ddot{\mathbf{q}}_i \end{bmatrix} \tag{33}$$

From Eqs. (23), (24) and (27) we get the following matrix relationship

$$\begin{bmatrix} \mathbf{q}_{i+1} \\ \dot{\mathbf{q}}_{i+1} \\ \ddot{\mathbf{q}}_{i+1} \end{bmatrix} = \mathbf{T} \begin{bmatrix} \mathbf{q}_{i+1}^* \\ \dot{\mathbf{q}}_{i+1}^* \\ \ddot{\mathbf{q}}_{i+1} \end{bmatrix}, \tag{34}$$

where matrix T is expressed in the block matrix form as

$$\mathbf{T} = \begin{bmatrix} \mathbf{I} & \mathbf{0} & \mathbf{I}\beta h^2 \\ \mathbf{0} & \mathbf{I} & \mathbf{I}\gamma h \\ \mathbf{0} & \mathbf{0} & \mathbf{I} \end{bmatrix} \tag{35}$$

The combination of Eqs. (28), (33) and (34) yields a new computational scheme for determining the solution of Eq. (2) at the time t_{i+1} in the form

$$
\begin{bmatrix} \mathbf{q}_{i+1} \\ \dot{\mathbf{q}}_{i+1} \\ \ddot{\mathbf{q}}_{i+1} \end{bmatrix} = \mathbf{T} \begin{bmatrix} & \mathbf{D} & \\ -(\mathbf{S}_{i+1})^{-1} \mathbf{H}_{i+1} \mathbf{D} \end{bmatrix} \begin{bmatrix} \mathbf{q}_i \\ \dot{\mathbf{q}}_i \\ \ddot{\mathbf{q}}_i \end{bmatrix} + \mathbf{T} \begin{bmatrix} \mathbf{0} \\ \mathbf{0} \\ (\mathbf{S}_{i+1})^{-1} \mathbf{d}_{i+1} \end{bmatrix}.
\tag{36}
$$

In this equation, the iterative computation is eliminated by introducing the direct solution for each time step. Note that T and D are matrices of constants.

By setting

$$
\mathbf{x}_i = \begin{bmatrix} \mathbf{q}_i \\ \dot{\mathbf{q}}_i \\ \mathbf{q}_i \end{bmatrix}, \qquad
\mathbf{A}_{i+1} = \mathbf{T} \begin{bmatrix} & \mathbf{D} & \\ -(\mathbf{S}_{i+1})^{-1} \mathbf{H}_{i+1} \mathbf{D} \end{bmatrix}, \qquad
\mathbf{b}_{i+1} = \mathbf{T} \begin{bmatrix} \mathbf{0} \\ \mathbf{0} \\ (\mathbf{S}_{i+1})^{-1} \mathbf{d}_{i+1} \end{bmatrix},
\tag{37}
$$

Eq. (36) can then be rewritten in the following form

$$
x_i = A_i x_{i-1} + b_i \quad (i = 1, \ 2, \ ..., \ m).
\tag{38}
$$

Expansion of Eq. (38) for $i = 1$ to m yields the same form as Eq. (20)

$$
\begin{aligned}
x_1 &= A_1 x_0 + c_1 \\
x_2 &= A_2 A_1 x_0 + c_2 \\
&................................ \\
x_m &= \left(\prod_{i=m}^{1} A_i \right) x_0 + c_m
\end{aligned}
\tag{39}
$$

where $c_0 = 0$, $c_1 = A_1 c_0 + b_1$, $c_2 = A_2 c_1 + b_2$,..., $c_m = A_m c_{m-1} + b_m$.

Using the condition of periodicity according to Eq. (22), the last equation of Eq. (39) yields a set of the linear algebraic equations

$$
\left(I - \prod_{i=m}^{1} A_i \right) x_0 = c_m.
\tag{40}
$$

The solution of Eq. (40) gives us the initial value for the periodic solution of Eq. (2). Finally, the periodic solution of Eq. (2) with the obtained initial value can be calculated without difficulties using the computational scheme in Eq. (36).

Based on the proposed numerical procedures in this section, a computer program with MATLAB to calculate periodic vibrations of transmission mechanisms has been developed and tested by the following application examples.

4. Application examples

4.1. Steady-state parametric vibration of an elastic cam mechanism

Cam mechanisms are frequently used in mechanical transmission systems to convert rotary motion into reciprocating motion (Figure 1). At high speed, the vibration of cam mechanisms causes transmission errors, cam surface fatigue, wear and noise. Because of that, the vibration problem of cam mechanisms has been investigated for a long time, both theoretically and experimentally.
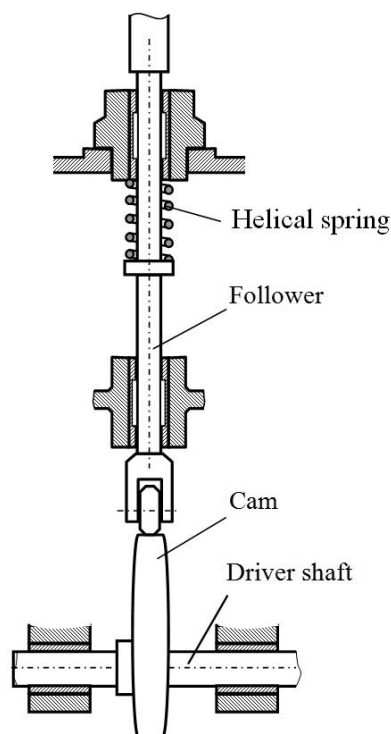

Figure 1. A cam mechanism.

The dynamic model of this system is schematically shown in Figure 2. This kind of model was also considered in a number of studies, e.g. [25-26]. The mechanical system of the elastic cam shaft, the cam with an elastic follower can be considered as rigid bodies connected by massless spring-damping elements with time-invariant stiffness k_i and constant damping coefficients c_i for $i = 1, 2, 3$. Among them k_1 is the torsional stiffness of the cam shaft. Parameter k_2 is the equivalent stiffness due to the longitudinal stiffness of the follower, the contact stiffness between the cam and the roller, and the cam bearing stiffness. Parameter k_3 denotes

the combined stiffness of the return spring and the support of the output link. The rotating components are modeled by two rotating disks with moments of inertia I_0 and I_1. Let us introduce into our dynamic model the nonlinear transmission function $U(\varphi_1)$ of the cam mechanism as a function of the rotating angle φ_1 of the cam shaft, the driving torque from the motor $M(t)$ and the external load $F(t)$ applied on the system.
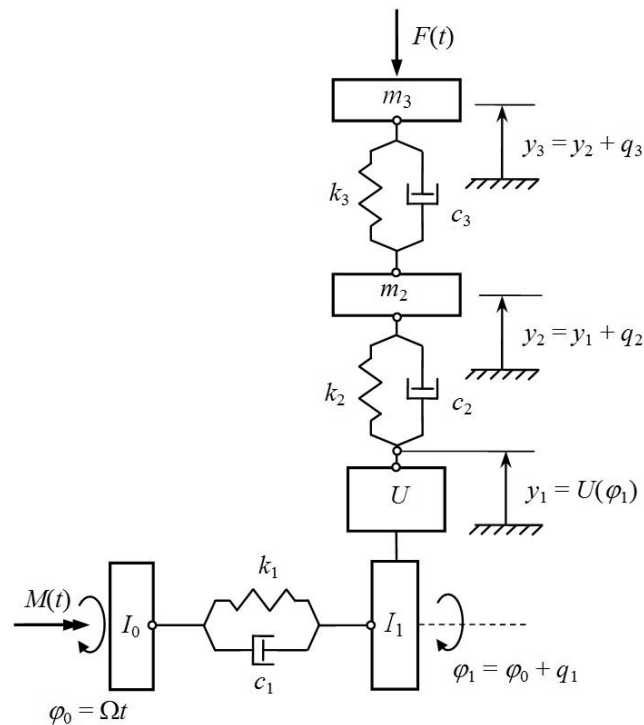

Figure 2. Dynamic model of the cam mechanism.

The kinetic energy, the potential energy and the dissipative function of the considered system can be expressed in the following form

$$T = \frac{1}{2}I_0\dot{\varphi}_0^2 + \frac{1}{2}I_1\dot{\varphi}_1^2 + \frac{1}{2}m_2\dot{y}_2^2 + \frac{1}{2}m_3\dot{y}_3^2 \tag{41}$$

$$\Pi = \frac{1}{2}k_1(\varphi_1 - \varphi_0)^2 + \frac{1}{2}k_2(y_2 - y_1)^2 + \frac{1}{2}k_3(y_3 - y_2)^2 \tag{42}$$

$$\Phi = \frac{1}{2}c_1(\dot{\varphi}_1 - \dot{\varphi}_0)^2 + \frac{1}{2}c_2(\dot{y}_2 - \dot{y}_1)^2 + \frac{1}{2}c_3(\dot{y}_3 - \dot{y}_2)^2 \tag{43}$$

The virtual work done by all non-conservative forces is

$$\sum \delta A = M(t)\delta\varphi_0 - F(t)\delta y_3 \tag{44}$$

Using the generalized coordinates φ_0, φ_1, q_2, q_3, we obtain the following relations

$$y_1 = U(\varphi_1), \quad y_2 = y_1 + q_2, \quad y_3 = y_2 + q_3 \tag{45}$$

Substitution of Eq. (45) into Eqs. (41-44) yields

$$T = \frac{1}{2}I_0\dot{\varphi}_0^2 + \frac{1}{2}I_1\dot{\varphi}_1^2 + \frac{1}{2}m_2(U'\dot{\varphi}_1 + \dot{q}_2)^2 + \frac{1}{2}m_3(U'\dot{\varphi}_1 + \dot{q}_2 + \dot{q}_3)^2, \tag{46}$$

$$\Pi = \frac{1}{2}k_1(\varphi_1 - \varphi_0)^2 + \frac{1}{2}k_2 q_2^2 + \frac{1}{2}k_3 q_3^2, \tag{47}$$

$$\Phi = \frac{1}{2}c_1(\dot{\varphi}_1 - \dot{\varphi}_0)^2 + \frac{1}{2}c_2\dot{q}_2^2 + \frac{1}{2}c_3\dot{q}_3^2, \tag{48}$$

$$\sum \delta A = M(t)\delta\varphi_0 - F(t)U'\delta\varphi_1 - F(t)\delta q_2 - F(t)\delta q_3, \tag{49}$$

where the prime represents the derivative with respect to the generalized coordinate φ_1. The generalized forces of all non-conservative forces are then derived from Eq. (49) as

$$Q_{\varphi_0}^* = M(t), \quad Q_{\varphi_1}^* = -F(t)U', \quad Q_{q_2}^* = -F(t), \quad Q_{q_3}^* = -F(t). \tag{50}$$

Substitution of Eqs. (46)-(48) and (50) into the Lagrange equation of the second type yields the differential equations of motion of the system in terms of the generalized coordinates φ_0, φ_1, q_2, q_3

$$I_0\ddot{\varphi}_0 - c_1(\dot{\varphi}_1 - \dot{\varphi}_0) - k_1(\varphi_1 - \varphi_0) = M(t), \tag{51}$$

$$\begin{aligned}
&[I_1 + (m_2 + m_3)U'^2]\ddot{\varphi}_1 + (m_2 + m_3)U'\ddot{q}_2 + m_3 U'\ddot{q}_3 + (m_2 + m_3)U'U''\dot{\varphi}_1^2 \\
&+ c_1(\dot{\varphi}_1 - \dot{\varphi}_0) + k_1(\varphi_1 - \varphi_0) = -F(t)U',
\end{aligned} \tag{52}$$

$$(m_2 + m_3)U'\ddot{\varphi}_1 + (m_2 + m_3)\ddot{q}_2 + m_3\ddot{q}_3 + (m_2 + m_3)U''\dot{\varphi}_1^2 + c_2\dot{q}_2 + k_2 q_2 = -F(t), \tag{53}$$

$$m_3 U'\ddot{\varphi}_1 + m_3\ddot{q}_2 + m_3\ddot{q}_3 + m_3 U''\dot{\varphi}_1^2 + c_3\dot{q}_3 + k_3 q_3 = -F(t). \tag{54}$$

When the angular velocity Ω of the driver input is assumed to be constant in the steady state

$$\varphi_0 = \Omega t, \tag{55}$$

one leads to the following relation

$$\varphi_1 = \Omega t + q_1, \tag{56}$$

where q_1 is the difference between rotating angles φ_0 and φ_1 due to the presence of the spring element k_1 and the damping element c_1. Assuming that φ_1 varies little from its mean value during the steady-state motion, the transmission function $y_1 = U(\varphi_1)$ depends essentially on the input angle $\varphi_0 = \Omega t$. Using the Taylor series expansion around Ωt, we get

$$U(\varphi_1) = U(\Omega t + q_1) = \overline{U} + \overline{U}' q_1 + \frac{1}{2}\overline{U}'' q_1^2 + \ldots, \tag{57}$$

$$U'(\varphi_1) = U'(\Omega t + q_1) = \overline{U}' + \overline{U}'' q_1 + \frac{1}{2}\overline{U}''' q_1^2 + \ldots, \tag{58}$$

$$U''(\varphi_1) = U''(\Omega t + q_1) = \overline{U}'' + \overline{U}''' q_1 + \frac{1}{2}\overline{U}^{(4)} q_1^2 + \ldots. \tag{59}$$

where we used the notations

$$\overline{U} = U(\Omega t), \ \overline{U}' = U'(\Omega t), \ \overline{U}'' = U''(\Omega t), \ \overline{U}''' = U'''(\Omega t). \tag{60}$$

Since the system performs small vibrations, i.e. there are only small vibrating amplitudes q_1, q_2 and q_3, substituting Eqs. (57)-(59) into Eqs. (52)-(54) and neglecting nonlinear terms, we obtain the linear differential equations of vibration for the system

$$\begin{aligned}
&\left(I_1 + (m_2 + m_3)\overline{U}'^2\right)\ddot{q}_1 + (m_2 + m_3)\overline{U}'\ddot{q}_2 + m_3\overline{U}'\ddot{q}_3 + \left[c_1 + 2(m_2 + m_3)\Omega\overline{U}'\overline{U}''\right]\dot{q}_1 \\
&+ \left[k_1 + F(t)\overline{U}'' + (m_2 + m_3)\Omega^2(\overline{U}'\overline{U}''' + \overline{U}''^2)\right]q_1 = -F(t)\overline{U}' - (m_2 + m_3)\Omega^2\overline{U}'\overline{U}'',
\end{aligned} \tag{61}$$

$$\begin{aligned}
&(m_2 + m_3)\overline{U}'\ddot{q}_1 + (m_2 + m_3)\ddot{q}_2 + m_3\ddot{q}_3 + 2(m_2 + m_3)\Omega\overline{U}''\dot{q}_1 \\
&+ c_2\dot{q}_2 + (m_2 + m_3)\Omega^2\overline{U}'''q_1 + k_2 q_2 = -F(t) - (m_2 + m_3)\Omega^2\overline{U}'',
\end{aligned} \tag{62}$$

$$m_3\overline{U}'\ddot{q}_1 + m_3\ddot{q}_2 + m_3\ddot{q}_3 + 2m_3\Omega\overline{U}''\dot{q}_1 + c_3\dot{q}_3 + m_3\Omega^2\overline{U}'''q_1 + k_3 q_3 = -F(t) - m_3\Omega^2\overline{U}''. \tag{63}$$

In most cases, the force $F(t)$ can be approximately a periodic function of the time or a constant. Thus, Eqs. (61)-(63) form a set of linear differential equations with periodic coefficients. Finally, the linearized differential equations of vibration can be expressed in the compact matrix form as

$$M(\Omega t)\ddot{q} + C(\Omega t)\dot{q} + K(\Omega t)q = d(\Omega t), \tag{64}$$

where

$$M(\Omega t) = \begin{bmatrix} I_1 + (m_2 + m_3)\overline{U}'^2 & (m_2 + m_3)\overline{U}' & m_3\overline{U}' \\ (m_2 + m_3)\overline{U}' & (m_2 + m_3) & m_3 \\ m_3\overline{U}' & m_3 & m_3 \end{bmatrix} \quad C(\Omega t) = \begin{bmatrix} c_1 + 2(m_2 + m_3)\Omega\overline{U}'\overline{U}'' & 0 & 0 \\ 2(m_2 + m_3)\Omega\overline{U}'' & c_2 & 0 \\ 2m_3\Omega\overline{U}'' & 0 & c_3 \end{bmatrix}$$

$$K(\Omega t) = \begin{bmatrix} k_1 + F\overline{U}'' + (m_2 + m_3)\Omega^2(\overline{U}'\overline{U}''' + \overline{U}''^2) & 0 & 0 \\ (m_2 + m_3)\Omega^2\overline{U}''' & k_2 & 0 \\ m_3\Omega^2\overline{U}''' & 0 & k_3 \end{bmatrix}$$

$$d(\Omega t) = \begin{bmatrix} -F\overline{U}' - (m_2 + m_3)\Omega^2\overline{U}'\overline{U}'' \\ -F - (m_2 + m_3)\Omega^2\overline{U}'' \\ -F - m_3\Omega^2\overline{U}'' \end{bmatrix}, \quad q = \begin{bmatrix} q_1 \\ q_2 \\ q_3 \end{bmatrix}.$$

We consider now the function $U'(\varphi)$, called the first grade of the transmission function $U(\varphi)$, where the angle φ is the rotating angle of the cam shaft. In steady state motion of the cam mechanism, function $U'(\varphi)$ can be approximately expressed by a truncated Fourier series

$$U'(\varphi) = \sum_{k=1}^{K} (a_k \cos k\varphi + b_k \sin k\varphi). \tag{65}$$

Parameters	Units	Values
m_2	(kg)	28
m_3	(kg)	50
I_1	(kgm^2)	0.12
k_1	(Nm/rad)	8×10^4
k_2	(N/m)	8.2×10^8
k_3	(N/m)	2.6×10^8
c_1	(Nms/rad)	18.5
c_2	(Ns/m)	1400
c_3	(Ns/m)	1200

Table 1. Calculation parameters.

The functions $\overline{U}'$, $\overline{U}''$, $\overline{U}'''$ in Eq. (64) can then be calculated using Eq. (65) for $\varphi = \Omega t$. Parameters used for the numerical calculation are listed in Table 1. Two set of coefficients a_k in Eq. (46) are given in Table 2 corresponding to two different cases of cam profile, coefficients $b_k = 0$. Without loss of generality, the external force F is assumed to have a constant value of 100 N.

a_k (m)	Case 1	Case 2
a_1	0.22165	0.22206
a_2	0	0
a_3	0.05560	0.08539
a_4	0	0
a_5	- 0.01706	0.00518
a_6	0	0
a_7	0	- 0.00373
a_8	0	0
a_9	0	0.00345
a_{10}	0	0
a_{11}	0	- 0.00182
a_{12}	0	0

Table 2. Fourier coefficients a_k of $U'(\varphi)$.
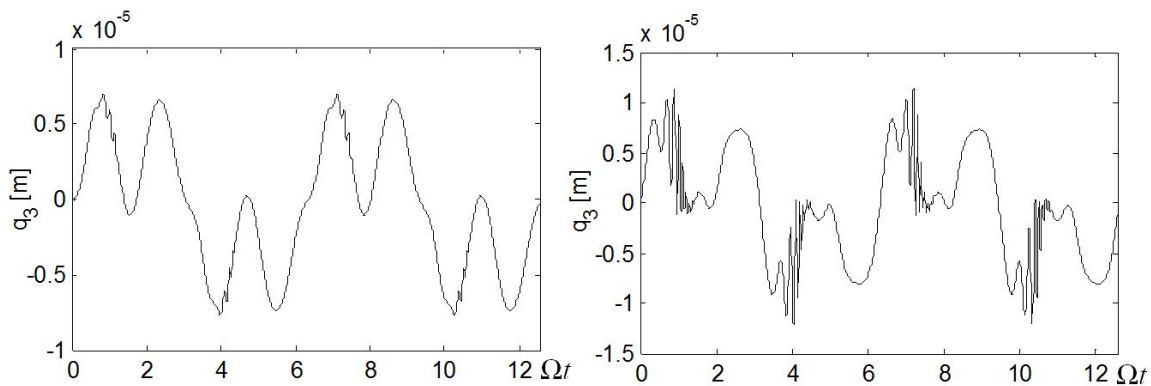
Figure 3. Dynamic transmission errors q_3 with n_{im}=100(rpm) for Case 1 (left) and Case 2 (right).

The rotating speed of the driver input n_{in} takes firstly the value of 100 (rpm) corresponding to angular velocity $\Omega \approx 10.47$ (rad/s) for the calculation. The periodic solutions of Eq. (64) are then calculated using the numerical procedures proposed in Section 3. The results of a periodic solution for coordinate q_3, which represents the dynamic transmission errors within the considered system, are shown in Figures 3 and 4. The influence of cam profile to the vibration response of the system can be recognized by a considerable difference in the vibration amplitude of both curves in Figure 3 and the frequency content of spectrums in Figure 4. In addition, the spectrums in Figure 4 shows harmonic components of the rotating frequency, such as ,Ω 3Ω, 5Ω which indicate stationary periodic vibrations.
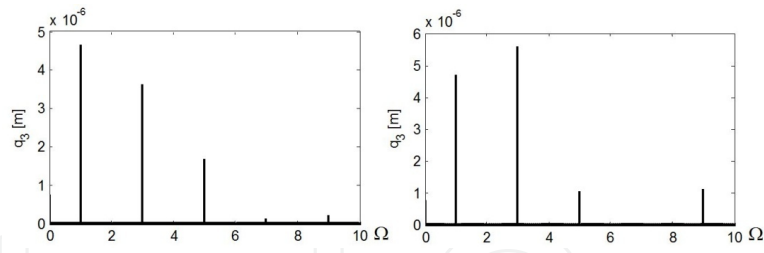
Figure 4. Frequency spectrum of q_3 with $n_{in} = 100(rpm)$ for Case 1 (left) and Case 2 (right).

Figures 5 and 6 show the calculating results with rotating speed $n_{in} = 600$ (rpm), corresponding to $\Omega \approx 62.8$ (rad/s). The mechanism has a more serious dynamic transmission error at high speeds. It can be seen clearly from the frequency spectrums that the steady state vibration at high speeds of the considered cam mechanism may include tens harmonics of the rotating frequency as mentioned in [3].
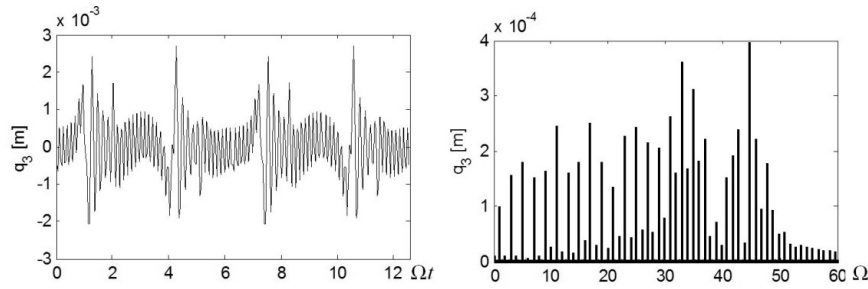
Figure 5. Dynamic transmission errors q_3 with $n_{in} = 600(rpm)$ for Case 1.
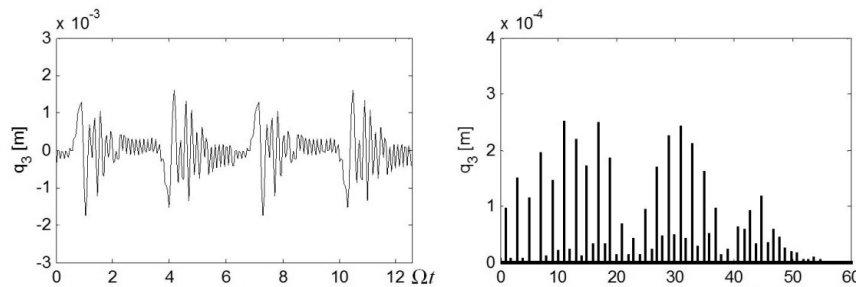
Figure 6. Dynamic transmission errors q_3 with $n_{in} = 600(rpm)$ for Case 2.

The calculation of the periodic solution of Eq. (64) was implemented by a self-written computer program in MATLAB environment, and a Dell Notebook equipped with CPU Intel® Core 2 Duo T6600 at 2.2 GHz and 3 GB memory. The calculating results obtained by the numerical procedures are identical, but the computation time with Newmark method is greatly reduced in comparison with Runge-Kutta method as shown in Figure 7, especially in the cases of large number of time steps.
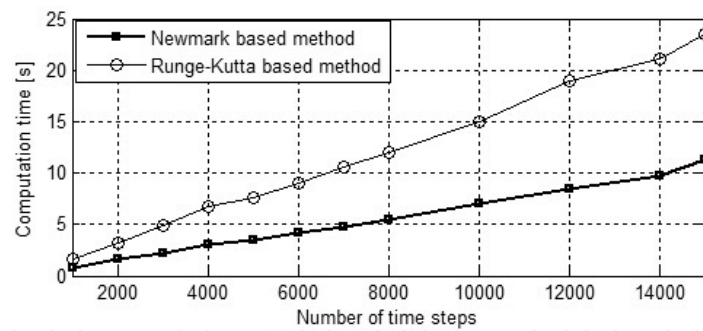
Figure 7. Comparison of the computation time for the model of cam mechanism.

4.2. Parametric vibration of a gear - pair system with faulted meshing

Dynamic modeling of gear vibrations offers a better understanding of the vibration genera-tion mechanisms as well as the dynamic behavior of the gear transmission in the presence of gear tooth damage. Since the main source of vibration in a geared transmission system is usually the meshing action of the gears, vibration models of the gear-pair in mesh have been developed, taking into consideration the most important dynamic factors such as effects of friction forces at the meshing interface, gear backlash, the time-varying mesh stiffness and the excitation from gear transmission errors [31-33].
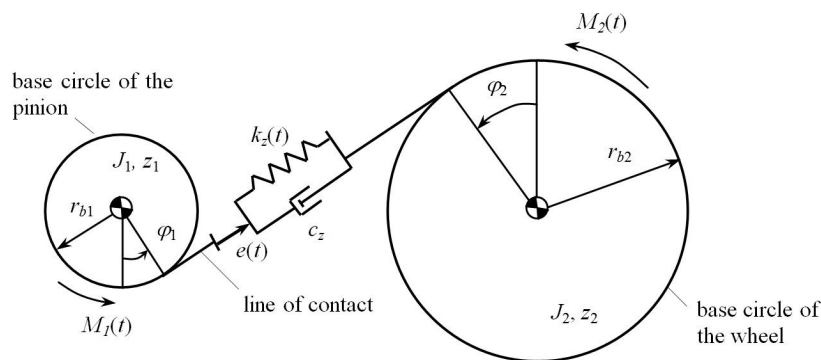

Figure 8. Dynamic model of the gear-pair system with faulted meshing.

From experimental works, it is well known that the most important components in gear vi-bration spectra are the tooth-meshing frequency and its harmonics, together with sideband structures due to the modulation effect. The increment in the number and amplitude of side-bands may indicate a gear fault condition, and the spacing of the sidebands is related to their source [27], [30]. However, according to our knowledge, there are in the literature only a few of theoretical studies concerning the effect of sidebands in gear vibration spectrum and the calculating results are usually not in agreement with the measurements. Therefore, the main objective of the following investigation is to unravel modulation effects which are responsible for generating such sidebands.

Figure 8 shows a relative simple dynamic model of a pair of helical gears. This kind of the model is also considered in references [24, 28, 32, 33]. The gear mesh is modeled as a pair of rigid disks connected by a spring-damper set along the line of contact.

The model takes into account influences of the static transmission error which is simulated by a displacement excitation $e(t)$ at the mesh. This transmissions error arises from several sources, such as tooth deflection under load, non-uniform tooth spacing, tooth profile errors caused by machining errors as well as pitting, scuffing of teeth flanks. The mesh stiffness $k_z(t)$ is expressed as a time-varying function. The gear-pair is assumed to operate under high torque condition with zero backlash and the effect of friction forces at the meshing interface is neglected. The viscous damping coefficient of the gear mesh c_z is assumed to be constant. The differential equations of motion for this system can be expressed in the form

$$J_1\ddot{\varphi}_1 + r_{b1}k_z(t)[r_{b1}\varphi_1 + r_{b2}\varphi_2 + e(t)] + r_{b1}c_z[r_{b1}\dot{\varphi}_1 + r_{b2}\dot{\varphi}_2 + \dot{e}(t)] = M_1(t), \tag{66}$$

$$J_2\ddot{\varphi}_2 + r_{b2}k_z(t)[r_{b1}\varphi_1 + r_{b2}\varphi_2 + e(t)] + r_{b2}c_z[r_{b1}\dot{\varphi}_1 + r_{b2}\dot{\varphi}_2 + \dot{e}(t)] = M_2(t). \tag{67}$$

where φ_i, $\dot{\varphi}_i$, $\ddot{\varphi}_i$ (i = 1,2) are rotation angle, angular velocity, angular acceleration of the input pinion and the output wheel respectively. J_1 and J_2 are the mass moments of inertia of the gears. $M_1(t)$ and $M_2(t)$ denote the external torques load applied on the system. r_{b1} and r_{b2} represent the base radii of the gears. By introducing the composite coordinate

$$q = r_{b1}\varphi_1 + r_{b2}\varphi_2. \tag{68}$$

Eqs. (66) and (67) yield a single differential equation in the following form

$$m_{red}\ddot{q} + k_z(t)q + c_z\dot{q} = F(t) - k_z(t)e(t) - c_z\dot{e}(t), \tag{69}$$

where

$$m_{red} = \frac{J_1J_2}{J_1r_{b2}^2 + J_2r_{b1}^2} \qquad F(t) = m_{red}\left(\frac{M_1(t)r_{b1}}{J_1} + \frac{M_2(t)r_{b2}}{J_2}\right). \tag{70}$$

Note that the rigid-body rotation from the original mathematical model in Eqs. (66) and (67) is eliminated by introducing the new coordinate $q(t)$ in Eq. (69). Variable $q(t)$ is called the dynamic transmission error of the gear-pair system [32]. Upon assuming that when $\dot{\varphi}_1 = \omega_1 = const$, $\dot{\varphi}_2 = \omega_2 = const$, $c_z = 0$, $k_z(t) = k_0$, the transmission error q is equal to the static tooth deflection under constant load q_0 as $q = r_{b1}\varphi_1 + r_{b2}\varphi_2 = q_0$. Eq. (69) yields the following relation

$$F(t) \approx F_0(t) = k_0q_0 + k_0e(t). \tag{71}$$

Eq. (69) can then be rewritten in the form

$$m_{red}\ddot{q} + k_z(t)q + c_z\dot{q} - f(t) = 0, \tag{72}$$

where $f(t) = k_0 q_0 - [k_z(t) - k_0]e(t) - c_z\dot{e}(t)$.

In steady state motion of the gear system, the mesh stiffness $k_z(t)$ can be approximately represented by a truncated Fourier series [33]

$$k_z(t) = k_0 + \sum_{n=1}^{N} k_n \cos(n\omega_z t + \gamma_n). \tag{73}$$

where ω_z is the gear meshing angular frequency which is equal to the number of gear teeth times the shaft angular frequency and N is the number of terms of the series.

In general, the error components are no identical for each gear tooth and will produce displacement excitation that is periodic with the gear rotation (i.e. repeated each time the tooth is in contact). The excitation function $e(t)$ can then be expressed in a Fourier series with the fundamental frequency corresponding to the rotation speed of the faulted gear. When the errors are situated at the teeth of the pinion, $e(t)$ may be taken in the form

$$e(t) = \sum_{i=1}^{I} e_i \cos(i\omega_1 t + \alpha_i). \tag{74}$$

Parameters	Pinion	Wheel
Gear type	helical, standard involute	
Material	steel	
Module (mm)	4.50	
Pressure angle (o)	20.00	
Helical angle (o)	14.56	
Number of teeth z	14	39
face width (mm)	67.00	45.00
base circle radius (mm)	30.46	84.86

Table 3. Parameters of the test gears.

Therefore, the vibration equation of gear-pair system according to Eq. (72) is a differential equation with the periodic coefficients.

According to the experimental setup which will be described later, the model parameters include $J_1 = 0.093$ (kgm^2), $J_2 = 0.272$ (kgm^2) and nominal pinion speed of 1800 rpm ($f_1 = 30$ Hz). The mesh stiffness of the test gear pair at particular meshing position was obtained by

means of a FEM software [29]. The static tooth deflection is estimated to be $q_0 = 1.2 \times 10^{-5}$ (m). The values of Fourier coefficients of the mesh stiffness with corresponding phase angles are given in Table 4. The mean value of the undamped natural frequency $\bar{\omega}_0 = \sqrt{k_0 / m_{red}} \approx 5462 \text{s}^{-1}$, corresponding to $\bar{f}_0 = \bar{\omega}_0 / 2\pi \approx 869$ (Hz). Based on the experimental work, the mean value of the Lehr damping ratio $\zeta = 0.024$ is used for the dynamic model. The damping coefficient c_z can then be determined by $c_z = 2\bar{\omega}_0 \zeta m_{red}$.

n	k_n(N/m)	γ_n(radian)
0	$8.1846 10^8$	
1	$3.2267 10^7$	2.5581
2	$1.3516 10^7$	-1.4421
3	$8.1510 10^6$	-2.2588
4	$3.5280 10^6$	0.9367
5	$4.0280 10^6$	-0.8696
6	$9.7100 10^5$	-2.0950
7	$1.4245 10^6$	0.9309
8	$1.5505 10^6$	0.2584
9	$4.6450 10^5$	-1.2510
10	$1.4158 10^6$	2.1636

Table 4. Fourier coefficients and phase angles of the mesh stiffness.

i	Case 1		Case 2	
	e_i(mm)	α_i(rad)	e_i(mm)	α_i(rad)
1	0.0015	-0.049	0.010	1.0470
2	0.0035	-1.7661	0.003	-1.4521
3	0.0027	-0.7286	0.0018	0.5233
4	0.0011	-0.5763	0.0011	1.4570
5	0.0005	-0.7810	0.0009	-0.8622
6	0.0013	1.8172	0.0003	1.1966

Table 5. Fourier coefficients and phase angles of excitation function $e(t)$.

Using the obtained periodic solutions of Eq. (72), the calculated dynamic transmission errors are shown in Figures 9 and 10 corresponding to different excitation functions $e(t)$ given in Table 5. The spectra in Figures 10(a) and 10(b) show clearly the meshing frequency and its harmonics with sideband structures. As expected, the sidebands are spaced by the rotational

frequency f_1 of the pinion. By comparing amplitude of these sidebands in both spectra, it can be concluded that the excitation function $e(t)$ caused by tooth errors is responsible for generating sidebands.
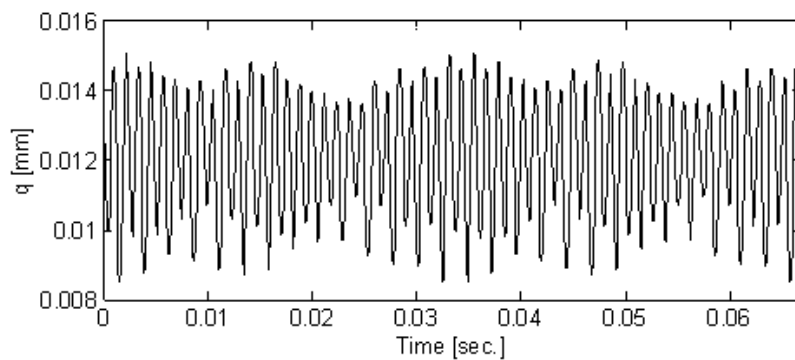

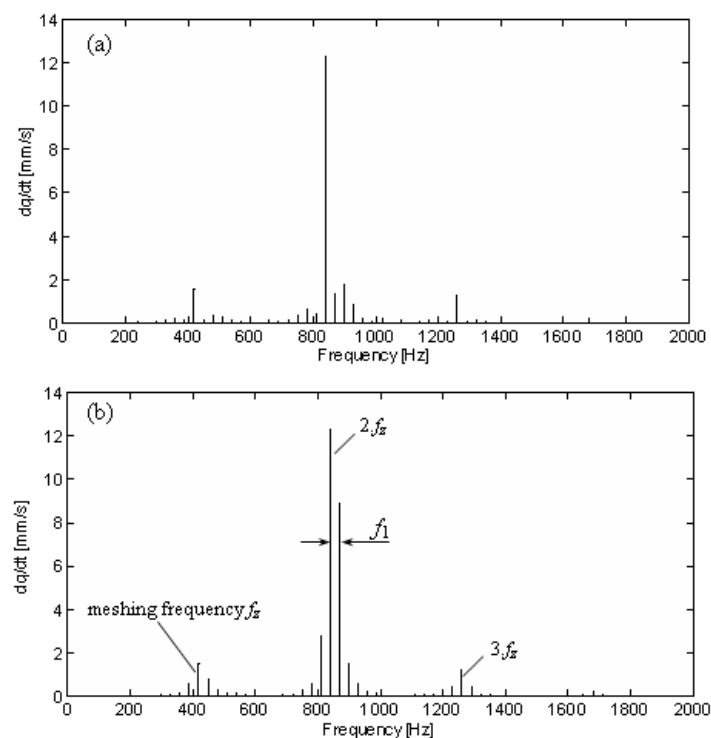**Figure 9.** . Modelling result: dynamic transmission error $q(t)$.

Figure 10. Modelling result: frequency spectrum of dq/dt corresponding to (a) excitation function $e(t)$ of Case 1 and b) excitation function $e(t)$ with larger coefficients (Case 2).

The experiment was done at an ordinary back-to-back test rig (Figure 11). The major param-eters of the test gear-pair are given in Table 3. The load torque was provided by a hydraulic rotary torque actuator which remains the external torque constant for any motor speed. The test gearbox operates at a nominal pinion speed of 1800 rpm. (30 Hz), thus the meshing fre-

quency f_z is 420 Hz. A Laser Doppler Vibrometer was used for measuring oscillating parts of the angular speed of the gear shafts (i.e. oscillating part of $\dot{\varphi}_1$ and $\dot{\varphi}_2$) in order to determine experimentally the dynamic transmission error. The measurement was taken with two non-contacting transducers mounted in proximity to the shafts, positioned at the closest position to the test gears. The vibration signals were sampled at 10 kHz. The signal used in this study was recorded at the end of 12-hours total test time, at that time a surface fatigue failure occurred on some teeth of the pinion.
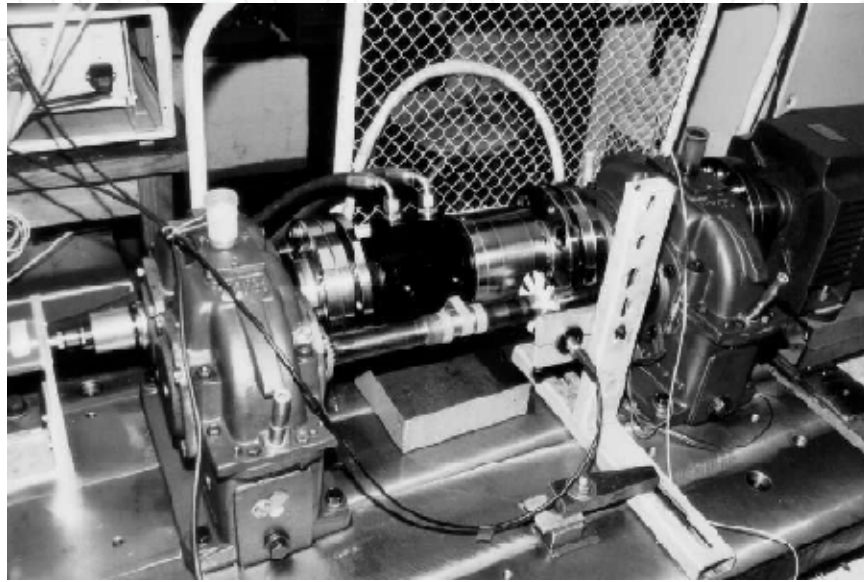
Figure 11. Gearbox test rig.
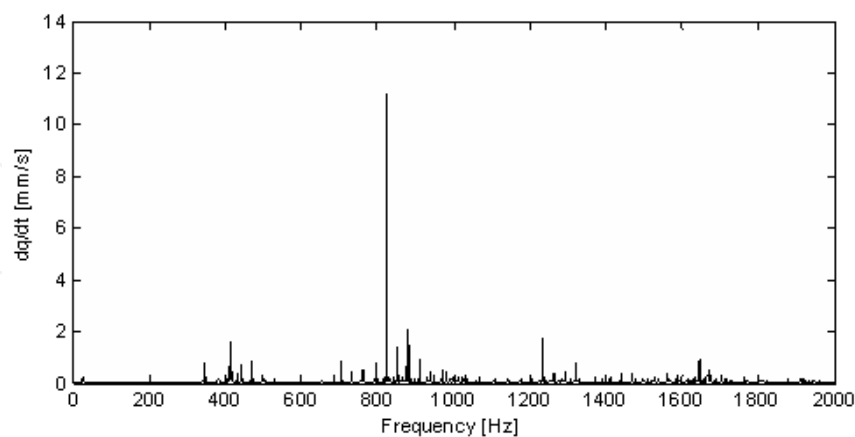
Figure 12. Experimental result: frequency spectrum of dq/dt.

Figure 12 shows a frequency spectrum of the first derivative of the dynamic transmission error $\dot{q}(t)$ determined from the experimental data. The spectrum presents sidebands at the meshing frequency and its harmonics. In particular, the dominant sidebands are spaced by

the rotational frequency of the pinion and characterized by high amplitude. This gives a clear indication of the presence of the faults on the pinion. By comparing the spectra displayed in Figures 13 and 14, it can be observed that the vibration spectrum calculated by numerical methods (Figure 13) and the spectrum of the measured vibration signal (Figure 14) show the same sideband structures.
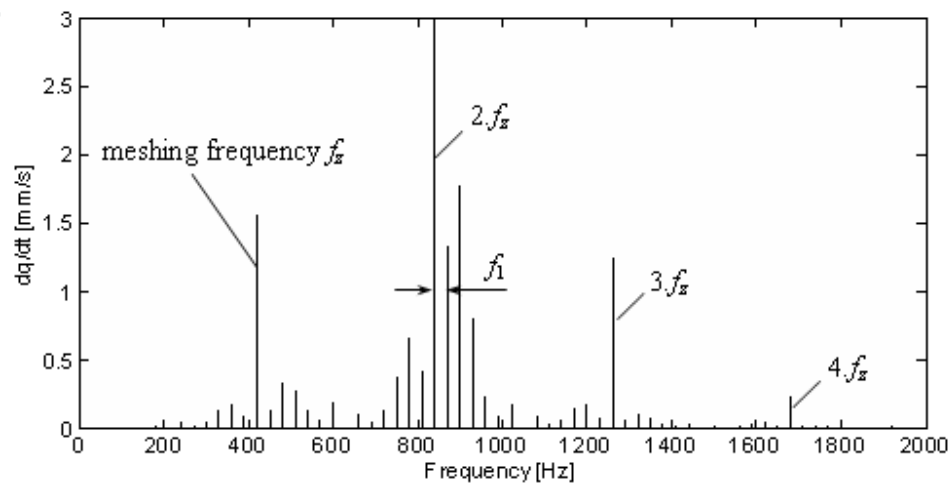

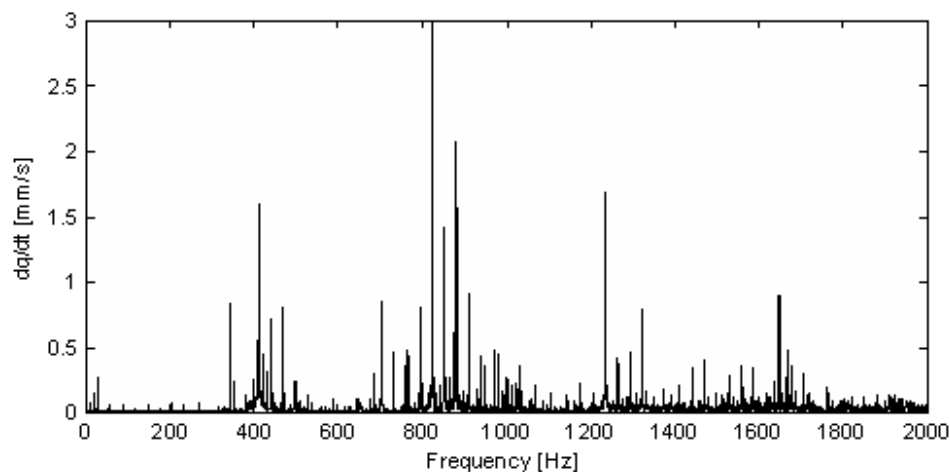**Figure 13.** Calculating result: frequency spectrum of dq/dt.

Figure 14. Experimental result: zoomed frequency spectrum of dq/dt from Figure 12.

The calculations required a large number of time steps to ensure that the frequency resolution in vibration spectra is fine enough. In comparison with the numerical procedure based on Runge-Kutta method, the computation time by the Newmark-based numerical procedure is greatly reduced for large number of time steps as shown in Figure 15, for that the same computer was used as in the previous example.
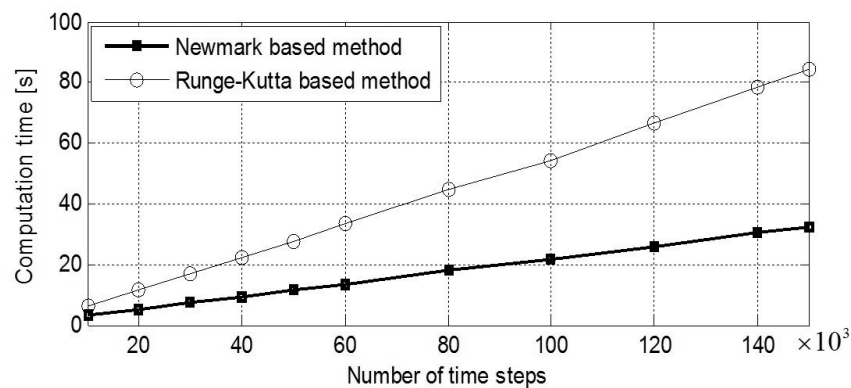
Figure 15. Comparison of the computation time for the gear-pair model.

4.3. Periodic vibration of the transport manipulator of a forging press

The most common forging equipment is the mechanical forging press. Mechanical presses function by using a transport manipulator with a cam mechanism to produce a preset at a certain location in the stroke. The kinematic schema of such mechanical adjustment unit is depicted in Figure 16.
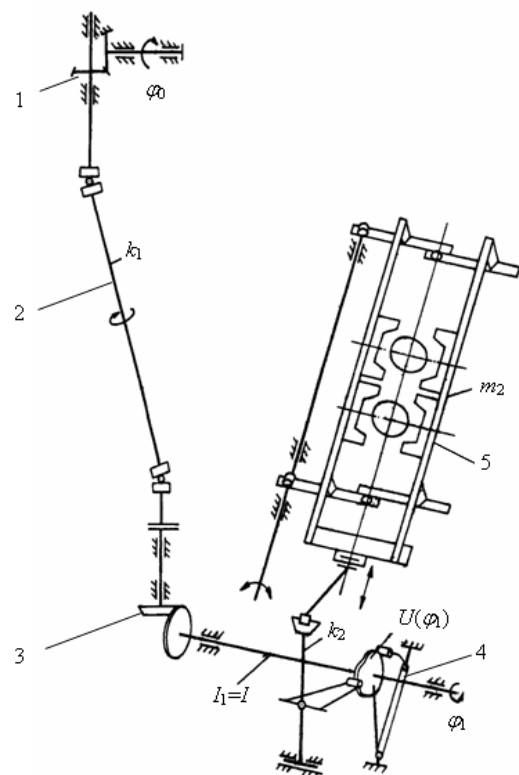

Figure 16. Kinematic schema of the transport manipulator of a forging press: 1- the first gearbox, 2- driving shaft, 3- the second gearbox, 4- cam mechanism, 5- operating mechanism (hammer).

The dynamic model of this system shown in Figure 17 is used to investigate periodic vibrations which are a commonly observed phenomenon in mechanical adjustment unit during the steady-state motion [18, 23]. The system of the driver shaft, the flexible transmission mechanism and the hammer can be considered as rigid bodies connected by spring-damping elements with time-invariant stiffness k_i and constant damping coefficients c_i, $i=1, 2$. The rotating components are modeled by two rotating disks with moments of inertia I_0 and I_1. The cam mechanism has a nonlinear transmission function $U(\varphi_1)$ as a function of the rotating angle φ_1 of the cam shaft, the driving torque from the motor $M(t)$ and the external load $F(t)$ applied on the system.
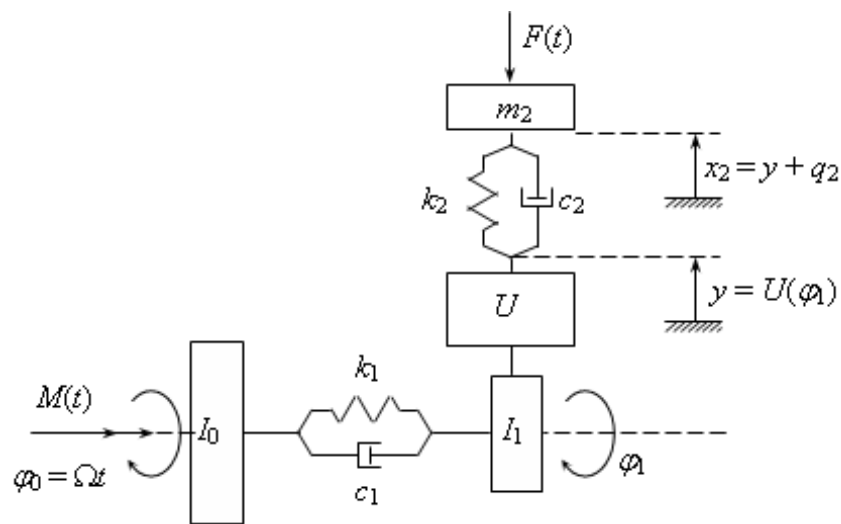

Figure 17. Dynamic model of the transport manipulator.

When the angular velocity Ω of the driver input is assumed to be constant in the steady state

$$\varphi_0 = \Omega t, \tag{75}$$

one leads to the following relation

$$\varphi_1 = \Omega t + q_1 \tag{76}$$

where q_1 is the difference between rotating angles φ_0 and φ_1 due to the presence of elastic element k_1 and damping element c_1, resulted from the flexible transmission mechanism.

By the analogous way as in Section 3.1, we obtain the linear differential equations of vibration for the system in the compact matrix form as

$$M(\Omega t)\ddot{q} + C(\Omega t)\dot{q} + K(\Omega t)q = d(\Omega t) \tag{77}$$

where

$$M(\Omega t) = \begin{bmatrix} I_1 + m_2\overline{U}'^2 & m_2\overline{U}' \\ m_2\overline{U}' & m_2 \end{bmatrix}, \ C(\Omega t) = \begin{bmatrix} c_1 + 2m_2\Omega\overline{U}'\overline{U}'' & 0 \\ 2m_2\Omega\overline{U}'' & c_2 \end{bmatrix}$$

$$K(\Omega t) = \begin{bmatrix} k_1 + F\overline{U}'' + m_2\Omega^2(\overline{U}'\overline{U}''' + \overline{U}''^2) & 0 \\ m_2\Omega^2\overline{U}''' & k_2 \end{bmatrix}, \ d = \begin{bmatrix} -F\overline{U}' - m_2\Omega^2\overline{U}'\overline{U}'' \\ -F - m_2\Omega^2\overline{U}'' \end{bmatrix}, \ q = \begin{bmatrix} q_1 \\ q_2 \end{bmatrix}$$

In steady state motion of the cam mechanism, function $U'(\varphi)$ takes the form [18, 23]

$$U'(\varphi) = \sum_{k=1}^{K} (a_k \cos k\varphi + b_k \sin k\varphi) \tag{78}$$

The functions $\overline{U}'$, $\overline{U}''$, $\overline{U}'''$ in Eq. (77) can then be calculated using Eq. (78) for $\varphi = \Omega t$.

The following parameters are used for numerical calculations: Rotating speed of the driver input n=50 (rpm) corresponding to Ω=5.236(1/s), stiffness k_1=7692 Nm; k_2=10^6 N/m, damping coefficients c_1=18.5 Nms; c_2=2332 Ns/m, I_1=1.11 kgm^2 and m_2=136 kg.
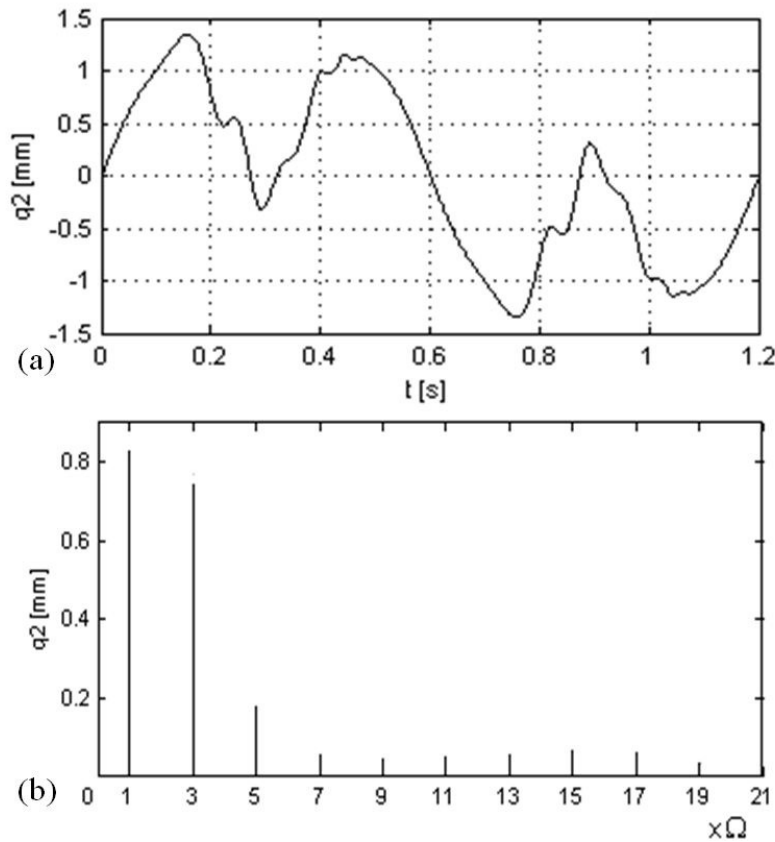

Figure 18. Calculating result of q_2 for case 1, (a) time curve, (b) frequency spectrum.
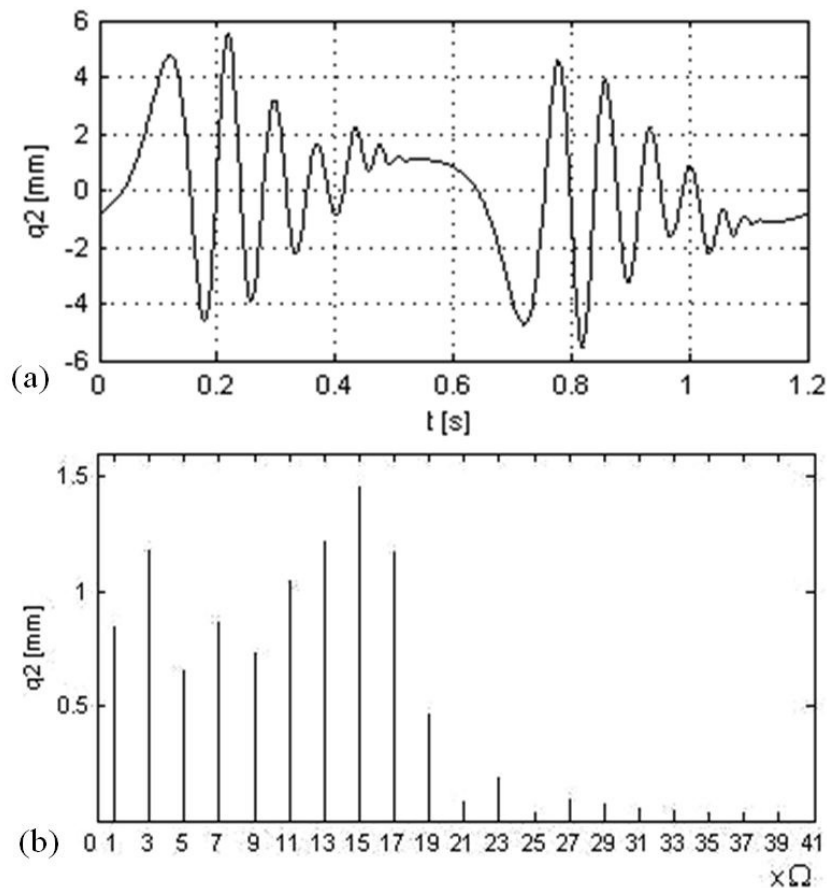
Figure 19. Calculating result of q_2 for case 2, (a) time curve, (b) frequency spectrum.

The Fourier coefficients a_k in Eq. (78) with $K = 12$ are given in Table 2 for two different cases and coefficients $b_k = 0$. We consider only periodic vibrations which are a commonly observed phenomenon in the system. The periodic solutions of Eq. (77) can be obtained by choosing appropriate initial conditions for the vector of variables q.

To verify the dynamic stable condition of the vibration system, the maximum of absolute value $|\rho|_{max}$ of the solutions of the characteristic equation, according to Eq. (10), is now calculated. The obtained values for both cases are $|\rho|_{max} = 0.001992$ (case 1) and $|\rho|_{max} = 0.001623$ (case 2). It can be concluded that the system is dynamically stable for both two cases since $|\rho|_{max} < 1$.

Calculating results of periodic vibrations of the mechanical adjustment unit, i.e. periodic solutions of Eq. (77), are shown in Figures 18-19 for two cases of the cam profile. Comparing both time curves, the influence of cam profiles on the vibration level of the hammer can be recognized. In addition, the frequency spectrums show harmonic components of the rotating frequency at Ω, 3Ω, 5Ω. These spectrums indicate that the considered system performs stationary periodic vibrations only.
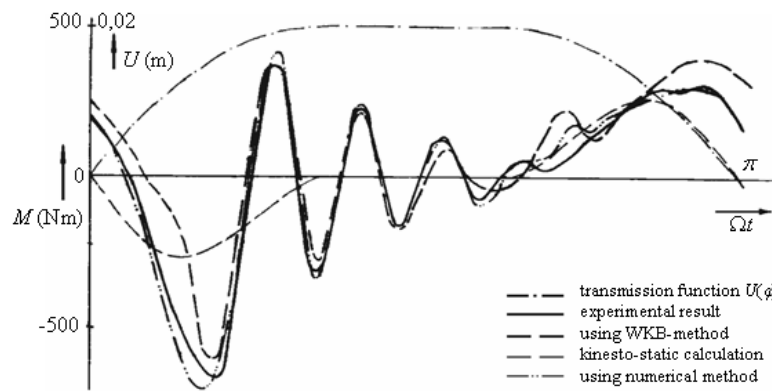
Figure 20. Dynamic moment acting on the driving shaft of the mechanical adjustment unit

To verify the calculating results using the numerical methods, the dynamic load moment of the mechanical adjustment unit was measured on the driving shaft (see also Figure 16). A typical record of the measured moment is plotted in Figure 20, together with the curves calculated from the dynamic model by using the WKB-method [18, 34], the kinesto-static calculation and the proposed numerical procedures based on Newmark method and Runge-Kutta method. Comparing the curves displayed in this figure, it can be observed that the calculating result using the numerical methods is more closely in agreement with the experimental result than the results obtained by the WKB-method and the kinesto-static calculation.

5. Concluding remarks

The calculation of dynamic stable conditions and periodic vibrations of elastic mechanisms and machines is an important problem in mechanical engineering. This chapter deals with the problem of dynamic modelling and parametric vibration of transmission mechanisms with elastic components governed by linearized differential equations having time-varying coefficients.

Numerical procedures based on Runge-Kutta method and Newmark integration method are proposed and applied to find periodic solutions of linear differential equations with time-periodic coefficients. The periodic solutions can be obtained by Newmark based procedure directly and more conveniently than the Runge-Kutta method. It is verified that the computation time with the Newmark based procedure reduced by about 60%-65% compared to the procedure using the fourth-order Runge-Kutta method (see also Figures 7 and 15). Note that this conclusion is only true for linear systems.

The numerical methods and algorithms are demonstrated and tested by three dynamic models of elastic transmission mechanisms. In the last two examples, a good agreement is obtained between the model result and the experimental result. It is believed that the proposed approaches can be successfully applied to more complicated systems. In addition, the proposed numerical procedures can be used to estimate approximate initial values for the shooting method to find the periodic solutions of nonlinear vibration equations.

Acknowledgements

Author details

Nguyen Van Khang[*] and Nguyen Phong Dien

*Address all correspondence to: nvankhang@mail.hut.edu.vn

Department of Applied Mechanics, Hanoi University of Science and Technology, Vietnam

References

[1] Schiehlen, W., & Eberhard, P. (2004). Technische Dynamik (2. Auflage). Stuttgart, B.G. Teubner.

[2] Shabana, A. A. (2005). Dynamics of multibody systems. 3. Edition). Cambridge, Cambridge University Press.

[3] Josephs, H., & Huston, R. L. (2002). Dynamics of mechanical systems. Boca Raton, CRS Press.

[4] Wittenburg, J. (2008). Dynamics of Multibody Systems. 4. Edition). Berlin, Springer.

[5] Stoer, J., & Bulirsch, R. (2000). Numerische Mathematik 2 (4. Auflage). Berlin, Springer.

[6] Newmark, N. M. (1959). A method of computation for structural dynamics. *ASCE Journal of Engineering Mechanics; Division*, 85-67.

[7] Géradin, M., & Rixen, D. (1994). Mechanical Vibrations. Chichester, Wiley.

[8] Nayfeh, A. H., & Balachandran, B. (1995). Applied nonlinear dynamics. New York, John Wiley & Sons.

[9] Eich-Soellner, E., & Fuehrer, C. (1998). Numerical Methods in multibody dynamics. Stuttgart, Teubner.

[10] Cesari, L. (1959). Asymptotic behaviour and stability problems in ordinary differential equations. Berlin, Springer.

[11] Jordan, D. W., & Smith, P. (2007). Nonlinear Ordinary differential equations. (4. Edition). New York, Oxford University Press.

[12] Kortüm, W., & Lugner, P. (1994). Systemdynamik und Regelung von Fahrzeugen. Berlin, Springer.

[13] Heimann, B., Gerth, W., & Popp, K. (2007). Mechantronik (3. Auflage). München, Fachbuchverlag Leipzig in Carl Hanser Verlag.

[14] Dresig, H., & Vulfson, I. I. (1989). Dynamik der Mechanismen. Berlin, Deutscher Verlag der Wissenschaften.

[15] Vulfson, I. I. (1973). Analytical investigation of vibration of mechanisms caused by parametric impulses. *Mechanism and Machine Theory*, 10, 305-313.

[16] Vulfson, I. I. (1989). Vibroactivity of branched and ring structured mechanical drives. New York, London: Hemisphere Publishing Corporation.

[17] Müller, P. C., & Schiehlen, W. (1976). Lineare Schwingungen. Wiesbaden, Akademische Verlagsgesellschaft.

[18] Nguyen , Van Khang. (1986). Dynamische Stabilität und periodische Schwingungen in Mechanismen. *Diss. B. TH Karl-Marx-Stadt*.

[19] Nguyen , Khang Van. (1982). Numerische Bestimmung der dynamischen Stabilitätsparameter und periodischen Schwingungen ebener Mechanismen. *Rev. Roum. Sci. Tech.-Mec. Appl*, 27(4), 495-507.

[20] Malkin, J. G. (1959). Theorie der Stabilät einer Bewegung. Berlin, Akademie.

[21] Troger, H., & Steindl, A. (1991). Nonlinear stability and bifurcation theory. Wien, Springer.

[22] Cleghorn, W. L., Fenton, R. G., & Tabarrok, B. (1984). Steady-state vibrational response of high-speed flexible mechanisms. *Mechanism and Machine Theory*, 417-423.

[23] Roessler, J. (1985). Dynamik von Mechanismen-Antriebssystemen im Textil- und Verarbeitungs-maschinenbau. *Diss. B. TH Karl-Marx-Stadt*.

[24] Nguyen, Van Khang, Thai, Manh Cau, & Nguyen, Phong Dien. (2004). Modelling parametric vibration of gear-pair systems as a tool for aiding gear fault diagnosis. *Technische Mechanik*, 24(3-4), 198-205.

[25] Volmer, J. (1989). Getriebetechnik/Kurvengetriebe . (2. Auflage). Berlin Verlag der Technik

[26] Nguyen, Van Khang, Nguyen, Phong Dien, & Vu, Van Khiem. (2010). Linearization and parametric vibration analysis of transmission mechanisms with elastic links. In: Proceedings of The First IFToMM Asian Conference on Mechanism and Machine Science Taipei, Taiwan

[27] Nguyen, Phong Dien. (2003). Beitrag zur Diagnostik der Verzahnungen in Getrieben mittels Zeit- Frequenz- Analyse. *Fortschritt-Berichte VDI; Reihe*, 11(135).

[28] Padmanabhan, C., & Singh, R. (1996). Analysis of periodically forced nonlinear Hill's oscillator with application to a geared system. *Journal of the Acoustial Society of America*, 99(1), 324-334.

[29] Boerner, J. (1999). Rechenprogramm LVR: Beanspruchungsverteilung an evolventischen Verzahnungen. *Foschungsberichte TU Dresden, Institut für Maschinenelemente und Maschinen-konstruktion.*

[30] Dalpiaz, G., Rivola, A., & Rubini, R. (2000). Effectiveness and sensitivity of vibration processing techniques for local fault detection in gears. *Mechanical System and Signal Processing*, 14(3), 387-412.

[31] Howard, I., Shengxiang, Jia., & Wang, J. (2001). The dynamic modelling of a spur gear in mesh including friction and a crack. *Mechanical System and Signal Processing*, 15(5), 831-853.

[32] Parker, G. R., Vijayakar, S. M., & Imajo, T. (2000). Non-linear dynamic response of a spur gear pair: Modelling and experimental comparisons. *J. Sound and Vibration*, 237(3), 435-455.

[33] Theodossiades, S., & Natsiavas, S. (2000). Non-linear dynamics of gear-pair systems with periodic stiffness and backlash. *J. Sound and Vibration*, 229(2), 287-310.

[34] Nguyen, Van Khang , Nguyen, Phong Dien, & Hoang , Manh Cuong. (2009). Linearization and parametric vibration analysis of some applied problems in multibody systems. *Multibody System Dynamics*, 22-163.